IEEE Access
Multidisciplinary | Rapid Review | Open Access Journal

Received 18 March 2026, accepted 4 April 2026, date of publication 13 April 2026, date of current version 29 April 2026.

Digital Object Identifier 10.1109/ACCESS.2026.3683582

RESEARCH ARTICLE

Evaluation of Support Vector Machine and Random Forest Models for EMG-Based Knee Motion Phase Classification

ING TECK PHANG[1], ASNOR JURAIZA ISHAK[1], (Senior Member, IEEE), SITI ANOM AHMAD[1], (Senior Member, IEEE), TOMOHIRO SHIBATA[2], (Member, IEEE), AND SLAMET RIYADI[3], (Member, IEEE)

[1]Department of Electrical and Electronic Engineering, Faculty of Engineering, Universiti Putra Malaysia (UPM), Serdang, Selangor 43400, Malaysia
[2]Kyushu Institute of Technology, Kitakyushu, Fukuoka 804-8550, Japan
[3]Department of Information Technology, Faculty of Engineering, Universitas Muhammadiyah Yogyakarta, Yogyakarta 55184, Indonesia

Corresponding author: Asnor Juraiza Ishak (asnorji@upm.edu.my)

This work was supported in part by the Universiti Putra Malaysia under the Putra Grant GP-GPB/2022/9712500.

ABSTRACT Knee-related conditions, such as anterior cruciate ligament injuries and meniscal ruptures, significantly affect mobility and quality of life. Although range-of-motion exercises are important for rehabilitation, interpreting electromyography signals related to these knee motions remains challenging owing to the complexity and variability of muscle activation patterns. This study investigated the classification of knee motion phases (resting, holding, and flexion/extension) by using surface electromyography signals from the biceps femoris and semitendinosus muscles in subjects with and without knee issues. Electromyography signals were preprocessed by removing outliers using the median absolute deviation and Kalman filtering. The motion phases were classified using a Support Vector Machine and Random Forest models within a subject-independent leave-one-subject-out evaluation framework. For subjects without knee issues, Random Forest performed with higher classification accuracy than Support Vector Machine for both muscles, with significant differences confirmed by McNemar's test ($p < 0.05$). For subjects with knee issues, both classifiers performed with comparable mean accuracies of approximately 90% for both muscles, with no statistically significant difference between models ($p > 0.05$), despite the Random Forest exhibiting slightly more temporally coherent time-series segmentation. The results demonstrate that electromyography-based motion phase classification is feasible under strict subject-independent evaluation. Random Forest showed greater robustness in healthy subjects, whereas both classifiers performed equivalently under pathological conditions, enhancing their potential application in intelligent rehabilitation and clinical motion assessment systems.

INDEX TERMS Electromyography signal, feature extraction, machine learning, random forest, signal classification, support vector machine.

I. INTRODUCTION

The knee plays an important role in daily routine by enabling movement, supporting body weight, and maintaining balance [1], [2]. Flexion and extension allow for limited lateral and minimal medial rotations. Hence, range of motion (ROM) exercises are important for enhancing circulation, reducing stiffness, and strengthening the surrounding muscles [3], [4]. As alpha motor neurons are responsible for conveying motor commands from the central nervous system, electromyography (EMG) signals provide information regarding muscle contractions [5], [6], [7], [8]. The quadriceps and hamstrings are the main stabilizers of the knee, with the hamstrings (biceps femoris, semitendinosus, and semimembranosus) contributing to flexion and extension movements [9], [10]. Muscle tension results from contractions triggered by motor

The associate editor coordinating the review of this manuscript and approving it for publication was Paolo Crippa.

signals. Gait involves a coordinated sequence of graded contractions and relaxations of the muscles in both lower limbs [11]. The EMG signal remains close to zero when the muscle is at rest or inactive [12]. During prolonged postures, the EMG signal increased and stabilized during knee extension. The EMG signal decreases as the knee flexes toward a 90-degree resting position [8]. The relationship between changes in flexion and extension angles and knee motion is illustrated in Fig. 1.

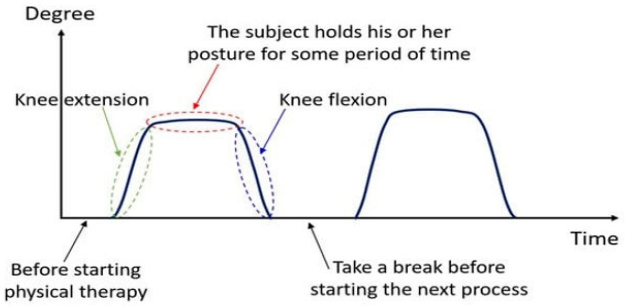

FIGURE 1. Angle changes with knee activities conducted [13].

Accurate EMG processing is important for classification because signals are complex and sensitive to noise. Kalman filters offer a computationally efficient solution for EMG signal processing. However, precise adjustments are required to prevent the loss of critical signal information [14], [15]. Kalman filters are superior to Butterworth and lowpass filters in preserving the original EMG waveform [16], [17], [18], [19]. When properly tuned, the Kalman filter keeps the temporal patterns of muscle activity more visible; thus, it clarifies activation patterns, optimizes feature extraction, and enhances classification performance.

Traditional EMG preprocessing commonly relies on fixed band-pass filtering [20], which effectively reduces broadband noise but neglects transient, high-amplitude spike artifacts arising from electrode motion, cable disturbances, and intermittent loss of skin–electrode contact [18]. These transient artifacts can distort short-term signal features and compromise the classifier robustness, particularly for dynamic and functional movements. Therefore, although band-pass and Butterworth filters are widely used, they do not explicitly address spike-induced contamination, which leads to misclassification and reduced reliability in EMG-based motion recognition systems.

Recent studies have shown that the application of Support Vector Machines (SVM) is highly effective in classifying EMG signals. The SVM can accurately differentiate complex patterns in muscle activity by defining the optimal hyperplane and applying kernel-based methods for feature separation. These approaches have consistently achieved classification accuracies exceeding 90% for tasks such as knee-angle prediction, hand-gesture recognition, and limb-movement classification [21], [22], [23]. The EMG datasets in these studies incorporated signals from the vastus lateralis, biceps femoris, gastrocnemius lateralis, semitendinosus, and tibialis anterior muscles, providing comprehensive insights into lower-limb kinematics [24]. Furthermore, previous research has recorded and interpreted two-channel surface EMG signals from the vastus lateralis and vastus medialis muscles using an EMG sensor during knee extension ROM monitoring [13]. In addition, a previous study classified ten finger movements using EMG signals from two arm sensors [25]. The Random Forest algorithm was implemented for feature selection according to the Gini importance. The model achieved a 97.5% accuracy in hand movement classification using the most significant features [25]. This study employed SVM and Random Forest algorithms to classify EMG signals, demonstrating strong accuracy and reliability [26], [27], [28].

Models such as artificial neural networks, support vector machines, random forest models, extreme learning machines, and linear discriminant analysis have demonstrated strong performances [29], [30]. The SVM achieved accuracies above 90% in classifying various EMG data for monitoring robotic manipulators [29], [30]. The random forest model achieved 96.3% accuracy in recognizing three simple hand gestures from 10 subjects by comparing the k-nearest neighbor (kNN), Discriminant Analysis (DA), Naïve Bayes (NB), and SVM classifiers. Random Forest classifier operates by designing multiple decision trees from random data samples and determines the final output through majority voting [30]. Convolutional Neural Networks (CNNs) have been employed as the core method for extracting spatial features from multi-channel and high-density EMG signals. Advanced approaches, such as LSTM and GRU, enable the capture of temporal dynamics of muscle activation sequences [31]. Transformer-based and attention-driven models exhibit a strong capability to manage long-range temporal dependencies and improve the generalization across different users. In addition, Graph Neural Networks (GNNs) are utilized to model the specific spatial relationships between electrodes, whereas multimodal fusion frameworks mitigate variability caused by changes in posture and session timing [31]. Despite their high performance, these deep models remain computationally intensive and often unsuitable for embedded and real-time applications. This limitation has motivated the development of lightweight, adaptive, and resource-efficient classification approaches [31], [32], [33].

Feature extraction includes waveform length, mean absolute value, root mean square (RMS), standard deviation, minimum, and maximum, with the latter two identified as the most significant [34]. The decision tree achieved 100% training, 99% testing, and 99% validation accuracy among the five classifiers, including linear discriminant analysis, logistic regression, decision tree, support vector machine, and k-nearest neighbor [35]. EMG signals from wearable sensors were used to classify the six activities using a random forest classifier for human activity recognition. The holdout method showed the highest accuracy, 82.08% from left–right biceps femoris signals, whereas running obtained 89.2% precision and 88.3% recall when both muscles were combined [36]. In addition, from the decomposed EMG signals, a set of

complementary features was extracted to capture the amplitude, temporal, and structural characteristics relevant to the muscle activation patterns. Specifically, the RMS value, fourth-order autoregressive (AR) model coefficients, waveform length, and wavelet-based features have been employed in previous studies [37], [38], [39].

Previous studies have demonstrated a strong linear relationship between the mean RMS value of EMG signals and corresponding muscle contraction amplitudes [40]. High correlations were observed at both the group and muscle levels, with particularly strong associations in the limbs. These findings indicate that RMS features reliably reflect subject-specific muscle activation [40]. Moreover, time-domain methods, such as AR modeling, capture the time-varying dynamics of the neuromuscular system during active contraction. The analysis highlighted that the prediction error variance of the AR model displays temporal trends that correlate with the muscle force production. They successfully differentiated healthy, neuropathic, and myopathic signals by estimating temporal trends using first-order regression [41]. Time–frequency techniques, specifically wavelet decomposition, address the nonstationary nature of muscle signals [18]. Wavelets allow the extraction of frequency-specific information while maintaining temporal alignment.

However, several recent EMG-based studies lack a detailed explanation of feature extraction and signal processing [42], [43]. Furthermore, previous EMG signal analyses lacked clarity in outlining the steps and features implemented for classification [21], [44]. This study proposes the development of a spike-aware EMG preprocessing framework that selectively removes transient impulsive artifacts using robust statistical detection and Kalman filtering, while preserving physiological muscle-activation dynamics to enhance feature-extraction and motion-phase classification accuracy. EMG data from individuals with and without knee issues were analyzed to establish a reliable baseline and evaluate the robustness of the model. Although deep learning approaches have shown high performance in EMG classification [31], these models are often limited by their reliance on large-scale datasets, high computational latency, and intensive hyperparameter optimization [33]. This makes it difficult to apply subject-independent scenarios and specific knee motion studies with limited data. Additionally, this study aimed to classify knee motion phases, specifically resting, holding, and flexion/extension, using EMG signals recorded from the biceps femoris and semitendinosus muscles and compared the performance of SVM and Random Forest classifiers across healthy and knee-impaired subjects.

The EMG preprocessing approach and feature extraction methods are described in Section II. A performance comparison between the Support Vector Machine and the Random Forest Classifier is provided in Section III, while the results are discussed in Section IV.

II. METHODOLOGY

A. EMG SIGNAL OF KNEE FLEXION AND EXTENSION

The EMG data utilized in this research were obtained from the UCI Machine Learning Repository and administered by Creative Commons Attribution 4.0, which allows the use of data with proper citations [45]. The dataset consisted of signal recordings from 22 male subjects aged 18 and above, with 11 individuals with knee issues, including anterior cruciate ligament (ACL) injuries, meniscal ruptures, and sciatica pain, and 11 without knee issues [46]. Data were collected from four surface electromyography (sEMG) channels, including the rectus femoris, biceps femoris, vastus medialis, and semitendinosus, along the goniometer channel. The subjects performed three physical tasks: walking, seated leg extension, and upward leg flexion. These tasks are common daily rehabilitation activities that do not require external equipment. The exercise focused on in this study was seated leg extension [45]. The sEMG signals were standardized to zero mean and unit variance to prevent overfitting and to accelerate model convergence during training.

In this study, surface EMG signals were recorded from the biceps femoris and semitendinosus muscles of both healthy subjects and subjects with knee-related issues to classify knee flexion/extension, resting, and holding phases. These two muscles were selected because they exhibit the most stable and distinct EMG signal patterns among the muscles evaluated in this study. Each dataset was required to contain observable cycles of resting, flexion/extension, and holding to identify temporal changes in EMG activity and meet the study requirements. The datasets had to be sufficiently long to fully represent complete movement cycles, particularly for the holding phase, which usually occurs over a short duration and is more difficult to map and affects classification accuracy. Datasets containing excessive spikes and artifacts that obscured the clarity of the motion cycles were excluded to ensure reliable classification of the flexion/extension and holding phases. For example, EMG recordings from the biceps femoris and semitendinosus muscles of the ninth and tenth healthy subjects were excluded because the datasets were insufficient in length and failed to exhibit clear cyclic patterns corresponding to resting, flexion/extension, and holding. Fig. 2a shows the EMG signal of the biceps femoris of Subject 9. These recordings exhibited relatively uniform energy levels, providing little meaningful information for classification. Semitendinosus muscle data from the second knee-related issue subject in Fig. 2b were excluded because of severe signal spikes that prevented reliable cycle interpretation. After applying the inclusion and exclusion criteria, 39 EMG datasets of the biceps femoris and semitendinosus muscles were obtained.

Motion-phase labels were generated using a data-driven, unsupervised labeling strategy. After spike removal and Kalman filtering, the EMG signal is segmented into fixed-length windows. The comprehensive feature set for each window was extracted, including time-domain statistics,

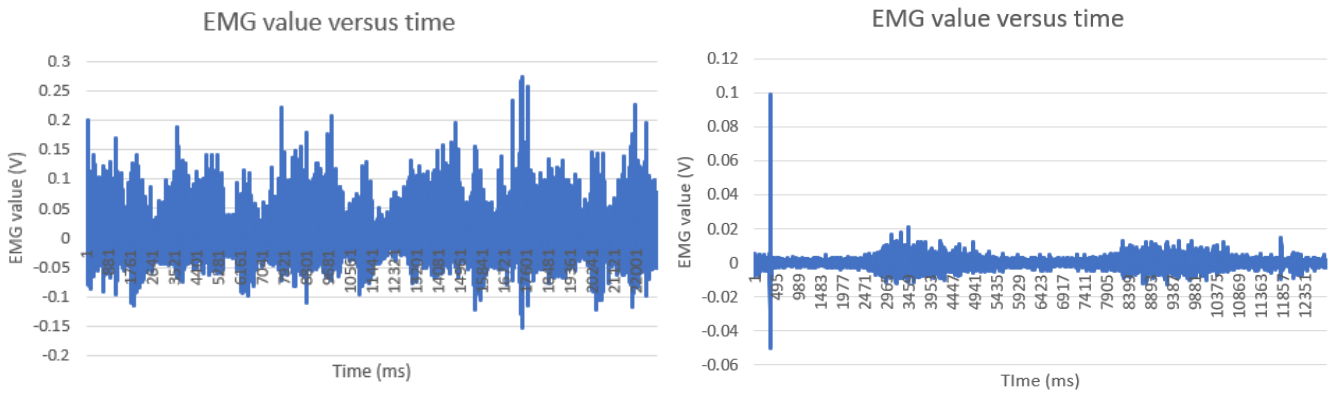

FIGURE 2. Representative EMG signals excluded from analysis: (a) Healthy Subject 9, (b) Knee-Issue Subject 2.

AR coefficients, and wavelet energy features to capture different aspects of muscle activation. K-means clustering (k = 3) was implemented only on the training windows to identify the distinct EMG activation patterns. These clusters were subsequently mapped to the resting, flexion/extension, and holding phases by ranking the cluster centroids based on the mean activation levels, with lower activation corresponding to rest and higher activation corresponding to movement-related states. The test windows were labeled by assigning them to the nearest training cluster centroid to avoid data leakage. The simple temporal constraints were the correct physiological transitions between phases, ensuring consistency with expected biomechanical motion sequences.

B. NOISE FILTERING VIA SPIKE REMOVAL AND KALMAN FILTERING

Before any simulation started, all previous outputs, variables, and figures were cleared to establish a controlled experimental environment, preventing residual data from influencing the subsequent analyses and visualizations. All random processes were initialized with a fixed seed to ensure consistent and repeatable results across the iterative runs.

High-amplitude impulsive spikes are frequently observed in surface EMG recordings in the dataset because of inherent noise sources such as motion artifacts, electromagnetic interference, and muscle crosstalk [47]. Although these artifacts are brief and non-physiological, failing to mitigate them can distort feature extraction and significantly degrade classification performance. A robust, window-based spike detection and interpolation strategy was employed. The EMG signal was segmented into non-overlapping windows of fixed length, consistent with the feature extraction window. Surface EMG signals were acquired at a sampling frequency of 1000 Hz, which was sufficient to capture the full spectral content of lower-limb muscle activity. Each window was processed independently to maintain the local signal statistics and avoid temporal smearing across segments. In this study, the window size was varied from 200 to 600 samples, with increments of 10 samples per trial, to determine the optimal window length. The maximum duration of transient impulse artifacts was evaluated at two thresholds, 10 and 20 samples, for each window size tested within the 200 to 600 sample range. However, when the EMG signal is free from noise and spikes, it can be analyzed using a wide range of window sizes. By contrast, the presence of significant noise and spikes restricts the range of usable window sizes.

Median absolute deviation (MAD_w) for each window in (1) was insensitive to large outliers. This property makes it suitable for EMG signals, in which large but sparse artifacts can inflate classical statistical measures and lead to excessive signal distortions.

$$\mathrm{MAD_w} = |\widetilde{x_w[n]} - \widetilde{x_w}| \tag{1}$$

$\widetilde{x_w}$ = The median of the EMG signal

The samples were labeled as abnormal when they surpassed the scaled MAD threshold defined in (2).

$$|\widetilde{x_w[n]} - \widetilde{x_w}| > 5 \text{ x } \mathrm{MAD_w} \tag{2}$$

A scaling factor of five was selected to ensure high sensitivity to impulsive artifacts while minimizing the risk of false detection of physiologically meaningful EMG bursts. This adaptive thresholding method automatically adjusts to local signal amplitude variations and eliminates the requirement of manually tuned global thresholds. The detected outlier samples were grouped into contiguous segments to isolate transient spikes from physiological muscle activity effectively. The identified spikes were replaced using piecewise cubic Hermite interpolating polynomial (PCHIP) interpolation based on neighboring valid samples. In standard spline techniques, the PCHIP interpolation preserves the natural morphology of the EMG signal without introducing an overshoot or oscillations. It can perform downstream feature extraction because the amplitude distortion introduced by conventional filtering methods can bias the features.

The Kalman filter minimizes the mean squared error when estimating the state of a dynamic system using noisy and uncertain measurements. It operates in two main phases:

prediction and update. In the prediction step, the filter estimates the next system state and its corresponding error covariance based on the previous state estimate and the system model. External control inputs were not considered for the EMG signal processing. Hence, only the state transition model and process noise are used to predict the state and error covariance.

In the update step, new measurement data were incorporated to refine the predicted state. Residual measurements were computed to determine the difference between actual and predicted measurements. The innovation covariance is calculated to account for the measurement uncertainty, followed by the computation of the Kalman gain. It balances the influence of the prediction and measurement. The predicted state estimate and error covariance were updated using the Kalman gain. The first-order Kalman filter attenuates residual high-frequency noise while retaining the temporal structure of the EMG signal.

The process noise covariance, Q, was set to a small fraction (0.001) of the signal variance to promote smooth temporal behavior while preventing excessive attenuation of true muscle activation.

The measurement noise covariance, R, was set proportional to the variance of the observed EMG signal (scaled by 0.1), representing the combined effects of sensor noise, motion artifacts, and residual interference. This choice ensures that the filter places greater confidence in the estimated latent state than in individual noisy measurements.

The relative scaling between Q and R (with $R \gg Q$) was selected to achieve stable smoothing behavior and preserve the EMG burst morphology while effectively reducing noise across all subjects. Because the Kalman filter was used solely as a preprocessing step rather than a predictive model, further parameter optimization was not performed to avoid overfitting and signal distortion.

C. NORMALIZATION AND FEATURE EXTRACTION

Knee motion is categorized into resting, flexion/extension, and holding at specific angles based on the EMG signal. Fig. 3 shows a flowchart of the EMG signal classification. Normalization using the min-max method scales the EMG data to the [0,1] range. This normalization promotes consistency among features without altering their relative magnitudes in (3) while also limiting the influence of outliers and placing all features on a common scale. Moreover, an appropriate window size is selected for the EMG signal, x, because different signals require different window lengths to achieve reliable classification.

Different datasets require appropriate window sizes for the classification. Although certain datasets achieve a high classification accuracy across multiple window sizes, others are restricted to a limited range. The usable window size

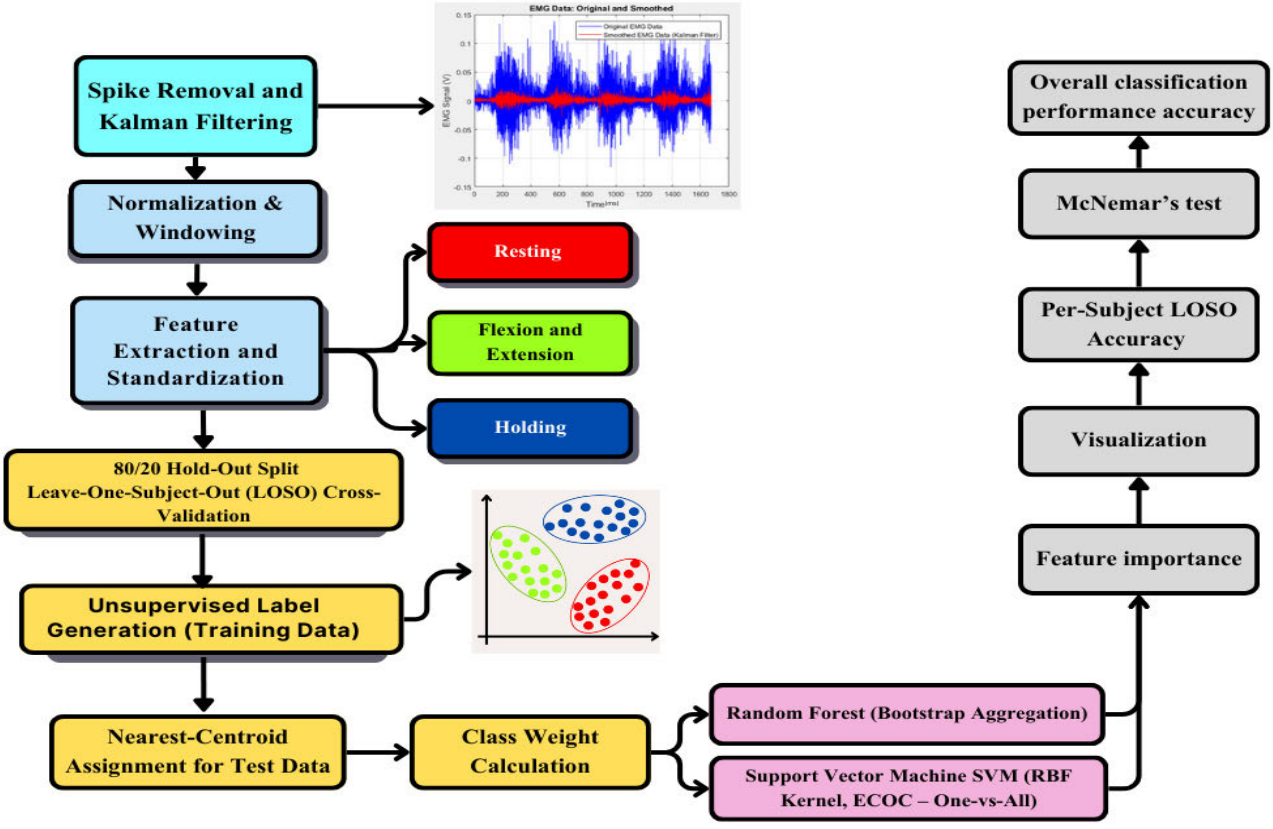

FIGURE 3. Flowchart of the classification of EMG signal using support vector machine (SVM) & random forest.

depends on the degree of the EMG signal fluctuation. Larger time windows help smooth out rapid variations, but obscure short muscle contractions. Smaller window sizes capture transient muscle bursts more accurately but increase sensitivity to noise. x_{no} implies the normalized EMG data.

$$x_{no} = \frac{x - \min(x)}{\max(x) - \min(x)} \tag{3}$$

Feature extraction involves transforming raw data into useful features that reflect the underlying structure of the muscle activity. The features applied in this study were the root mean square (RMS), standard deviation, maximum and minimum values, robust minimum (5th percentile), waveform length, autoregressive (AR) model coefficients (order 4), and wavelet-based energy features (order 4).

RMS (Feature 1) provides a stable estimate of the EMG amplitude and is robust to zero-mean fluctuations. During rest, RMS values were minimal, while holding, RMS remained moderate and stable. During flexion/extension, RMS increases notably because of dynamic muscle activation. The standard deviation (Feature 2) represents the variability in the muscle activity related to dynamic contractions. A high standard deviation indicated greater fluctuations in muscle activity, particularly in relation to movement and transitions. Conversely, a low standard deviation indicates steadier muscle states, such as holding and resting.

The maximum value (Feature 3) is aligned with bursts of muscle activity, such as strong contractions during intense muscle actions. The maximum value detects moments of high exertion, particularly during rapid muscle contraction. These are characteristic of the flexion/extension phases.

The minimum value classifies periods of minimal muscle activity, whereas the true minimum is highly sensitive to residual noise and artifacts. The 5th percentile (Feature 4) offers a robust lower-bound estimate of the baseline activity, enhancing stability across subjects and trials.

Waveform length (Feature 5) indicates the cumulative length of the EMG signal within a window. More intense activities, such as sustained contractions, result in a higher waveform length compared with less active and relaxed states. A low waveform length is a strong indicator of muscle stability when differentiating between flexion/extension and resting phases.

The AR model of order four (features 6-9) offers an effective trade-off between the representational power and overfitting. AR coefficients capture variations in signal dynamics across different motion phases without requiring an explicit Fourier-based analysis. Equation (4) shows the windowed EMG signal sample at a discrete time index, $x_w[n]$, model order, p, AR coefficients, a_k, log index, k, and residual noise, $e[n]$.

$$x_w[n] = \sum_{k=1}^{p} a_k x_w[n-k] + e[n], p = 4 \tag{4}$$

The Discrete Wavelet Transform (features 10-13) using the Daubechies-4 (db4) wavelet decomposes the EMG signal into multiple frequency subbands, enabling joint time–frequency analysis. The energy of each subband reflects frequency-specific muscle activation patterns: low-frequency components correspond to sustained contractions, while high-frequency components represent rapid muscle activation during flexion/extension. Flexion and extension use the same features and patterns during classification; therefore, they were not classified in this study.

Each EMG window is represented by a 13-dimensional feature vector consisting of amplitude-based features (RMS, maximum value, and robust minimum at the 5th percentile), variability and complexity measures (standard deviation and waveform length), parametric spectral descriptors (AR coefficients), and time–frequency energy features (wavelet subband energies). The different motion phases exhibited distinct EMG signatures:

- Resting:
  Low RMS, low standard deviation, minimal waveform length, and low wavelet energy across all bands
- Holding:
  Moderate RMS, low variability, stable AR coefficients, and dominant low-frequency wavelet energy
- Flexion/Extension:
  High RMS, high standard deviation, waveform length, distinct AR patterns, and elevated high-frequency wavelet energy

The feature importances of SVM and Random Forest was visualized through graphs to understand the contribution of each feature to EMG signal classification across different models. Because the SVM classifier utilizes a nonlinear Radial Basis Function (RBF) kernel, the resulting model lacks explicit feature weights for direct interpretation. Feature relevance randomly shuffles the values of a single feature in the test set while keeping all others constant and measures the decrease in classification accuracy. The features that caused the most significant decline in performance were identified as the primary drivers of the decision-making process of the model.

Random Forest calculates feature importance by measuring the contribution of each feature to reduce the classification error. It uses permutation importance, where the values of a feature are shuffled, and the increase in prediction error is measured, as shown in (5). T is the number of trees in the ensemble. $\Delta E_{f,t}$ represents the increase in error caused by permutation feature (f) in tree (t). Feature importance was averaged over all trees in the forest to provide a reliable assessment. An increase in error upon permuting a feature indicates that the feature is more important for accurate classification.

$$\text{Importance}_{\text{f}} = \frac{1}{T} \sum_{t=1}^{T} \Delta E_{f,t} \tag{5}$$

D. STANDARDIZATION OF FEATURES AND K-MEANS CLUSTERING

Standardization (z-score scaling) transforms each feature to have a mean of zero and standard deviation of 1. This enabled

each feature to contribute equally to the model. Larger-scales features could dominate the analysis without standardization, preventing the model from detecting meaningful patterns. This process improves the performance of machine learning algorithms by eliminating the bias caused by varying the feature scales. This helps the gradient-based optimization methods converge more efficiently.

The EMG feature windows were split before clustering and model training using a time-ordered hold-out strategy. All overlapping windows remained within the same range. The dataset was partitioned sequentially without shuffling. The first 80% of the time-ordered windows were used for training, and the remaining 20% were reserved for testing. Feature extraction in (6) was performed using non-overlapping windows of a fixed length, ensuring that the adjacent samples were statistically independent and that no raw EMG samples were shared between the training and testing sets. x_k is the feature vector, L is the window length, and k is the window index.

$$x_k = \emptyset(x_w\,[k-1]\,L{+}1 : kL]) \tag{6}$$

The Leave-One-Subject-Out (LOSO) cross-validation strategy was applied to ensure that the model evaluation reflects genuine generalization across individuals. Each subject was completely excluded from training once, and testing was performed on this subject. This prevents shared EMG statistics, muscle patterns, or motion signatures from affecting the classifier. This ensures that the evaluation reflects true generalization across individuals.

The motion-phase labels were generated using a data-driven unsupervised labeling strategy applied exclusively to the training data. K-means clustering was performed with K=3, based on physiological considerations of lower-limb EMG activity. No test samples were included in the clustering process, thereby preventing any form of label leakage or information transfer from the evaluation set. Within each subject, the feature windows may overlap, but LOSO ensures that no overlapping windows exist between subjects, thereby avoiding cross-subject leakage. Centroids for clustering and statistical normalization were computed and limited to training subjects, and the test subjects remained completely unseen.

The resulting groups were mapped to meaningful motion-phase classes based on the mean EMG activation level of each cluster centroid. Clusters were categorized based on their average activity levels, such that the cluster with the lowest mean activation was assigned to resting, the intermediate cluster to holding, and the highest-activation cluster to movement in (7). This mapping introduces physiological interpretability rather than supervision. This ensured that the final evaluation was untainted and unbiased by keeping the test data separate. $\mu_{k,m}$ is the m-th component of the centroid vector for cluster k, d is the feature dimensionality, and m is the feature index.

$$\overline{\mu_k} = \frac{1}{d}\sum_{m=1}^{d}\mu_{k,m} \tag{7}$$

Each test feature vector was categorized by mapping it to the nearest training centroid using the minimum-distance criterion. The test data remained completely unseen, thereby removing label leakage and maintaining the integrity of the evaluation protocol by freezing centroids learned from the training set. The feature vector for the i-th data point is assigned to cluster j. Equation (8) shows the formula for cluster j, where μ_k is the centroid of the kth cluster. x_i is the data point.

$$j = \text{argmin}_k\,|\,|x_i - \mu_k|\,|^2 \tag{8}$$

Once the motion-phase labels were established, supervised classifiers (SVM and Random Forest) were trained using the labeled training data. Model evaluation was conducted using a held-out test set. This design produced a clear two-stage learning pipeline: (1) unsupervised, physiologically grounded label generation using training data only, followed by (2) supervised classification and unbiased testing. This structural separation ensures that the high classification accuracy reflects genuine model generalization rather than being inflated by data leakage, clustering bias, or incidental correlations between sets. Let the dataset be denoted as

$$D = \{(x_i, y_i)\}_{i=1}^{N}, \tag{9}$$

where y_i denotes the corresponding motion-phase label.

The dataset is partitioned into distinct training and testing subsets. Inverse-frequency class weighting is applied within the SVM optimization to recognize the imbalanced distribution of motion phases in EMG data as resting states occur more frequently than active states. This approach assigns higher penalties for misclassifying minority classes, such as holding and dynamic movements. This prevents the model from developing a bias toward the dominant resting phase. The classifier achieved more balanced performance and maintained a greater number of classifiers.

Equation (10) delineates the weighted loss minimization in the SVM. ξ_i is a slack variable that allows misclassification. C is a regularization parameter that calibrates the trade-off between margin maximization and error minimization. w_i represents the class-dependent weight assigned to each sample and is typically derived from the inverse frequency of each class. Misclassification errors from minority classes incur more substantial penalties than those from the majority of resting classes.

$$\min_{W,\xi}\frac{1}{2}|\,|w|\,|^2 + C\sum_{i=1}^{N} w_i\xi_i \tag{10}$$

$$\text{subject to}: \; y_i\left(w^T x_i + b\right) \geq 1 - \xi i, \; \xi_i \geq 0 \tag{11}$$

Both classifiers employed inverse-frequency class weighting to handle the naturally imbalanced distribution of motion phases in EMG data. These weights were embedded into both the SVM and Random Forest training objectives, ensuring that the minority motion phases (holding) retained their diagnostic significance and are not overshadowed by the dominant resting class.

Systematic hyperparameter tuning was performed by using a held-out validation strategy. Hyperparameter optimization was performed on the training data, whereas the final assessment was conducted on the unseen test set. The box constraint parameter C $\in$ {0.1,1,10} and kernel scale $\in$ {0.1,1,10} for the SVM classifier were systematically explored. The trained model was evaluated by using a held-out test set for each hyperparameter combination. The configuration with the highest classification accuracy is selected as the optimal model. Furthermore, the Random Forest classifier was evaluated by varying the number of decision trees {50,100,200}. Each forest used bootstrap aggregation with majority voting for the final predictions, ensuring a fair and consistent comparison across both the classification frameworks.

E. SUPPORT VECTOR MACHINE (SVM) AND RANDOM FOREST

The classification framework leverages SVMs to identify an optimal hyperplane for class separation. The input data are mapped into a high-dimensional feature space, allowing the decision boundary to be implicitly defined by support vectors rather than by an explicit weight vector by employing kernel functions. The error-correcting output code (ECOC) approach trains multiclass models by decomposing multiclass problems into multiple binary classification problems and increasing the accuracy and error tolerance. Each binary classifier was trained using a specific subset of the dataset, and its individual outputs were subsequently integrated to produce the final prediction. SVM uses the one-vs-all method to learn a hyperplane for each class. Multiclass classification decomposes the three-class problem into multiple binary SVM classifiers by using a one-versus-all strategy. All binary classifiers evaluate the sample, and the class with the highest confidence is selected. The SVM model uses each feature vector, applies a decision function, and assigns it to the class with the highest score among the binary classifiers.

Random Forest creates multiple decision trees and combines their predictions to enhance the classification accuracy and reduce overfitting. Decision trees recursively split data into subsets based on feature values, with each internal node representing a decision and each leaf node representing a class label. The criteria for splitting nodes in decision trees are the Gini index and the entropy. Equation (12) calculates the Gini index at node. p_i denotes the probability of class i at node. The Gini index calculates the impurity level of a node. It reaches 0 when all samples belong to one class (pure) and reaches a maximum when the classes are evenly distributed. A high Gini index indicates a lack of clear separation, suggesting that the resulting split offers minimal information gain. Conversely, a lower Gini index signifies a greater node purity, confirming that the selected feature effectively discriminates between classes and yields a more homogenous partition.

$$\text{Gini} = 1 - \sum_{i=1}^{k} p_i^2 \tag{12}$$

Node entropy, as defined in Equation (13), provides a quantitative measure of the information gain achieved at each split. Entropy equals 0 as the node achieves perfect homogeneity. The elevated entropy levels signify a high degree of class diversity, requiring further splittings to reduce the uncertainty within the EMG signal classification.

$$\text{Entropy} = \sum_{i=1}^{k} p_i \log_2 (p_i) \tag{13}$$

A random subset of the training data is selected by replacement to train each tree. If there were N samples in total, each tree was trained on N samples. At each split in the tree, only a random subset of features is evaluated at each decision node. This dual-randomization strategy ensures that each tree remains unique. Random Forest aggregates these independent predictions through a majority voting consensus in (14).

$$\hat{y} = \text{mode}\,(h_1\,(x)\,, \ldots, h_T\,(x) \tag{14}$$

Random Forest is equally robust when configured for regression tasks. The model generates a continuous output by calculating the arithmetic mean of all the individual tree predictions in (15). Ensemble averaging effectively reduces the variance and stabilizes the final estimate.

$$\hat{y} = \frac{1}{T} \sum_{j=1}^{T} h_j(x) \tag{15}$$

The Random Forest model utilizes bootstrap sampling to cultivate an ensemble of diverse learners, which collectively predict class labels for each input sample. Predictions are made through averaging, making Random Forest resilient against overfitting and effective for EMG signal classification. Class weights were embedded into the SVM hinge-loss objective and Random Forest split criteria. This adjustment neutralized the inherent bias toward the dominant resting state. Both models were trained using identical LOSO splits with the same features. This standardization ensures that any performance disparities are a direct consequence of the underlying model architecture rather than artifacts in the data distribution.

F. PERFORMANCE EVALUATION

The Random Forest and SVM models were compared through a multi-faceted assessment, utilizing the feature importance and performance data detailed in Table 1. The McNemar test was employed to ensure that the observed differences in accuracy represented statistically significant shifts in predictive behavior rather than random variation.

III. RESULTS AND DISCUSSION

The EMG signal dataset was collected from subjects with and without knee issues. Representative subjects from each group were selected to illustrate the comparison between the original and filtered signals, feature importance analysis, and performance comparison between the SVM and Random Forest classifiers. For all 39 subjects, the biceps femoris and semitendinosus muscles were analyzed and presented in terms of per-subject LOSO accuracy, overall classification

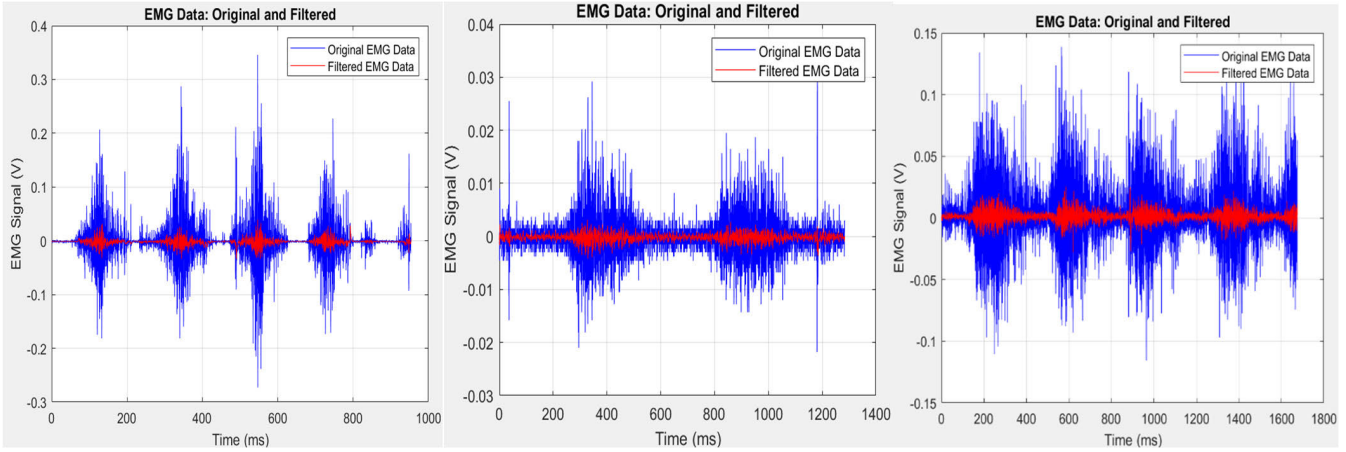

FIGURE 4. Comparison between the original and filtered EMG signal: (a) Healthy subject 3, (b) Knee-Issue subject 2, (c) Knee-Issue subject 10.

TABLE 1. Result presentation format.

Result element	Display format
Original vs filtered EMG comparison	Figures
Feature importance	Bar plot
SVM vs Random Forest comparison	Figures
Per-Subject LOSO Accuracy	Figures
Overall classification performance accuracy	Tables (mean ± standard deviation)
McNemar's test	Text

accuracy, and statistical significance evaluated using McNemar's test.

A. COMPARISON OF ORIGINAL AND FILTERED EMG SIGNALS

Fig. 4 shows the original and filtered EMG signals for different subjects. Three subjects were selected for comparison of the filtered EMG signal with the original EMG signal. EMG data for subjects 3 and 10 were obtained from the semitendinosus muscle, whereas data for subject 2 were acquired from the biceps femoris muscle. The median absolute deviation estimates the dispersion without being influenced by the spikes. Most spikes and noise were removed because the median absolute deviation-based outlier rejection eliminated impulsive artifacts, whereas the Kalman filter attenuated stochastic high-frequency noise through recursive optimal state estimation. Thresholding at $5 \times$ MAD flags only extreme deviations, which detects impulsive artifacts and replaces them using local shape-preserving interpolation. The Kalman filter attenuates Gaussian noise, minor fluctuations, and high-frequency jitter, thereby creating a smoother signal while suppressing high-frequency signals.

B. SUBJECT WITHOUT KNEE ISSUES FOR THE BICEPS FEMORIS AND SEMITENDINOSUS MUSCLE

Based on Fig. 5, the feature importance distributions obtained from the SVM and Random Forest models were highly similar; therefore, only one representative feature importance plot was presented for different subjects.

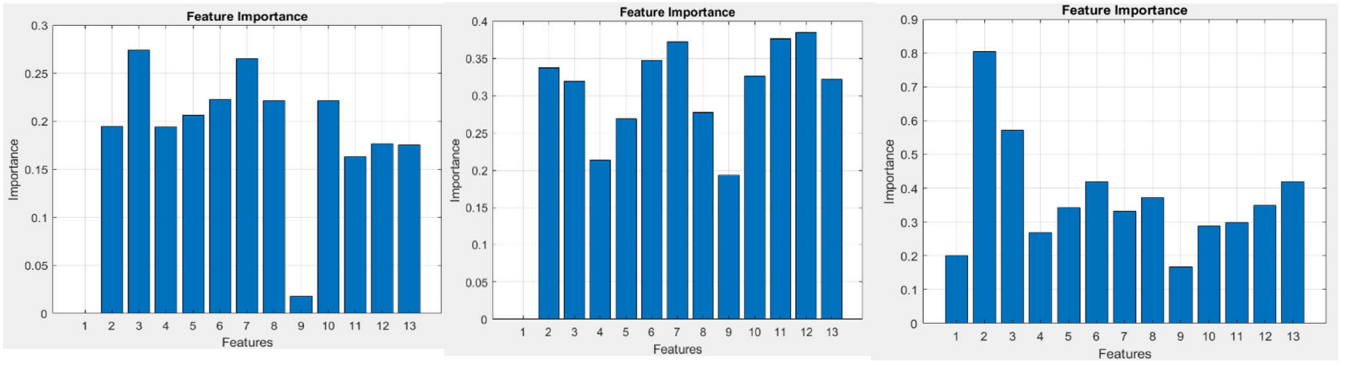

FIGURE 5. Feature importance of healthy subject: (a) semitendinosus subject 1, (b) semitendinosus subject 3, (c) biceps femoris subject 4.

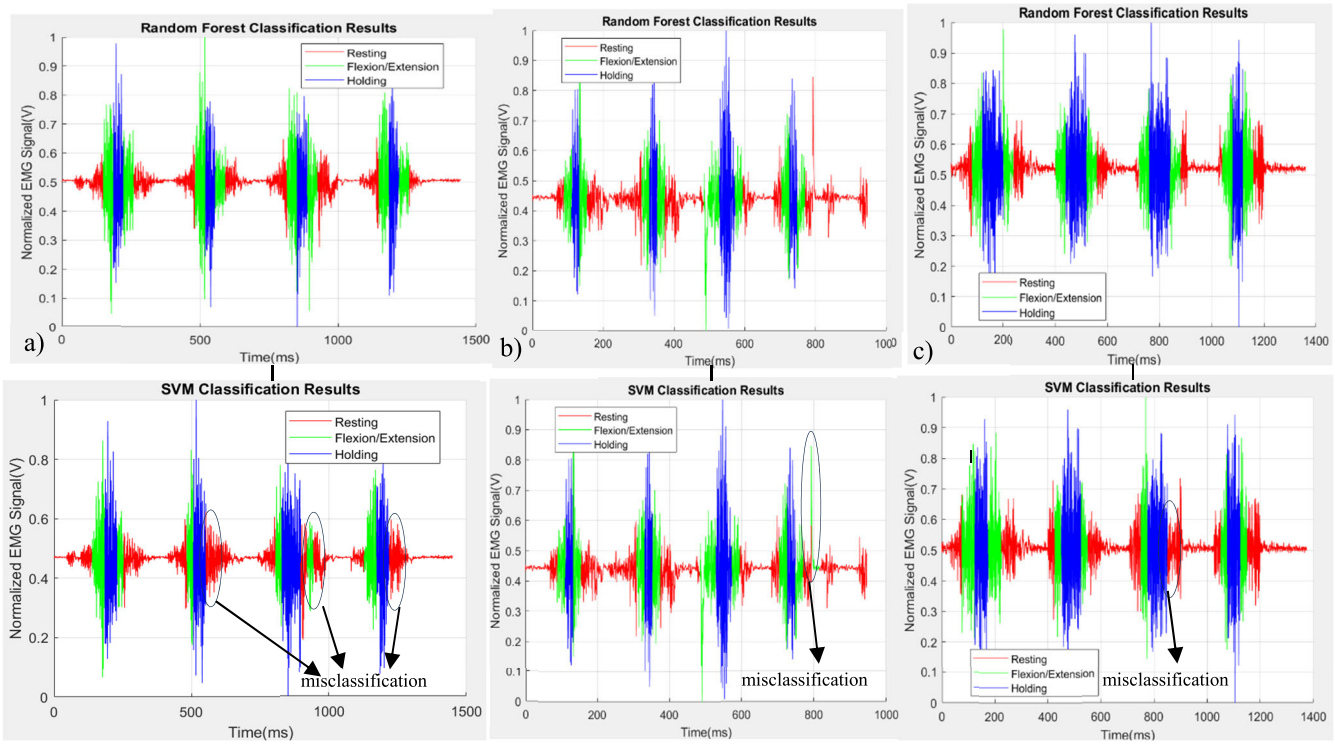

FIGURE 6. Comparison between random forest and SVM: (a) semitendinosus subject 1, (b) semitendinosus subject 3, (c) biceps femoris subject 4.

Feature importance reflects the contribution of each feature to the classifier's decision-making process. Muscle activation patterns exhibit significant inter-subject variability, driven by unique signal characteristics. As illustrated in Figs. 5a and 5b, the feature importance distribution was relatively balanced, indicating that the classifier leveraged a synergistic combination of descriptors rather than a single dominant variable. Motion phases are separable through the multi-dimensional representations of amplitude, temporal, and spectral data. However, the RMS value and AR coefficients showed lower importance scores owing to the similar average muscle activation levels across motion phases and the limited differences in short-term temporal dynamics between classes.

Fig. 5c reveals that Feature 2 (standard deviation) emerged as the primary contributor to classification of the motion phases. Subject 4 demonstrated a clearer separation between the holding, resting, and flexion/extension phases, likely due to highly distinct motion transitions. Subject 4 exhibited more well-defined motion phases than those in Figs. 5a and 5b, which contained more noise during classification, resulting in improved discriminative clarity. The time-series comparison in Fig. 6 maps the SVM and Random Forest predictions directly onto the normalized EMG signal. The plots highlight different signal segments, colored based on the predicted class, such as resting, flexion/extension, and holding, providing insight into muscle activity dynamics over time. These figures show a direct comparison between the models, showing that each model classifies various EMG segments.

As illustrated in Fig. 6, the SVM model misclassifies a small fraction of the flexion/extension phase as the resting phase. In addition, a minor portion of the resting phase is misidentified as an active flexion/extension. This clustering overlap highlights a subtle boundary ambiguity between the minimal active movement and the true static phases. The Random Forest model performed better, with more accurate and distinct segmentation of the EMG signal phases, making it more suited for the task than the SVM model. The Random Forest model demonstrates a more accurate and stable classification, with a clear segmentation between the activity and non-activity states. The transitions between classes were more aligned with expected muscle activity patterns.

TABLE 2. LOSO classification accuracy and MCNEMAR'S test results for SVM and random forest.

	Models	Biceps femoris	Semitendinosus
Overall classification performance accuracy	SVM	81.79% ± 12.10	75.99% ± 15.58
	Random forest	88.59% ± 9.30	82.50% ± 13.49
McNemar's test		0.0422	0.0072

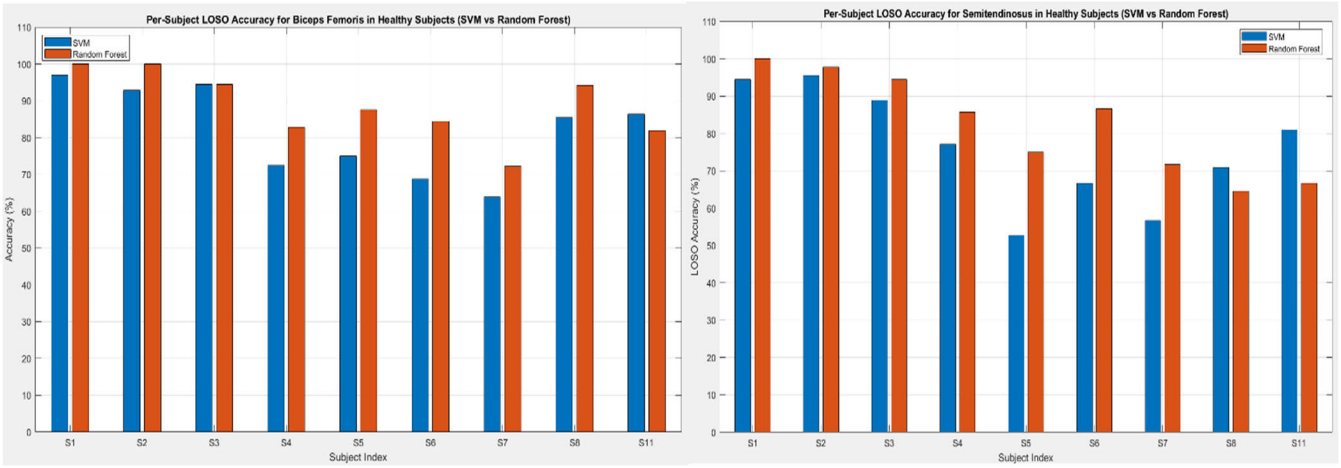

FIGURE 7. Per-subject LOSO Accuracy (a) biceps femoris (b) semitendinosus.

Joint angle measurements were used solely to derive physiologically meaningful motion-phase labels, whereas classification accuracy was computed by comparing the EMG-based predictions against these angle-derived reference labels.

Certain subjects exhibited lower classification accuracy owing to signal noise and discrepancies between the EMG-based classification and corresponding joint angle measurements. While the recorded joint-angle signals are smooth and exhibit minimal fluctuation, EMG signals reflect the underlying neuromuscular activation, which does not always directly correspond to joint kinematics or limb position. Consequently, EMG activity varies even when the joint angle remains constant, leading to unavoidable misclassifications in certain motion phases. This physiological mismatch between muscle activation and joint kinematics contributes to the classification ambiguity and highlights the inherent challenges of EMG-based motion phase recognition.

The lower standard deviation observed for Random Forest indicates more stable generalization across subjects, whereas the larger variability for SVM suggests greater sensitivity to inter-subject EMG differences. The Random Forest consistently outperformed the SVM for both muscles, achieving higher mean accuracy and lower inter-subject variability (Table 2). McNemar's test revealed statistically significant differences between the classifiers for both muscles ($p < 0.05$), confirming that the observed performance gains were not attributable to chance. These results demonstrate the robustness of Random Forest for EMG-based motion phase classification in subject-independent settings.

Fig. 7 shows the per-subject LOSO accuracy for the semitendinosus and biceps femoris. Accuracy was computed solely by comparing the predicted labels with angle-derived labels at the window level. It is used only to generate motion-phase labels, which are then treated as ground-truth targets to evaluate classification accuracy. Joint angle signals were used for motion-phase labeling and were not provided as input features to the classifiers. Across both muscles, Random Forest achieved higher mean classification accuracy than SVM under the subject-independent LOSO evaluation protocol.

C. SUBJECT WITH KNEE ISSUES FOR THE BICEPS FEMORIS AND SEMITENDINOSUS MUSCLE

Figs. 8a and 8b demonstrate a relatively uniform distribution of feature importance, indicating that the classification relies on a combination of multiple features. The comparatively lower contribution of the RMS and fourth-order AR coefficient is attributed to the similar mean activation levels across motion phases. Fig. 8c reveals a pronounced dominance of standard deviation, implying that the EMG signal variability differs substantially between motion phases, thereby enhancing its discriminative power.

The time-series plots in Fig. 9 compare the predictions of the SVM and Random Forest models for the normalized EMG signal. Different segments of the signal are colored according to the predicted class, representing muscle activity over time. This visualization facilitates side-by-side assessment of the two models to distinguish between physiological rest and active muscle states. SVM incorrectly classified a small segment of the flexion/extension phase as the holding phase. A minor portion of the resting phase is misidentified as active flexion/extension. The Random Forest model shows coherent segmentation and is more accurate at classifying different states (Resting, Holding, Flexion/Extension) than the SVM model, making it better suited for the task. The divergence in the results highlights the advantage of Random Forest ensemble-based voting over SVM hyperplane optimization when processing complex, imbalanced signal characteristics inherent in this study.

The performance of SVM remains highly contingent on the precise calibration of the kernel function, regularization parameters, and class-weighting schemes. Random Forest demonstrates superior handling of non-linear dependencies

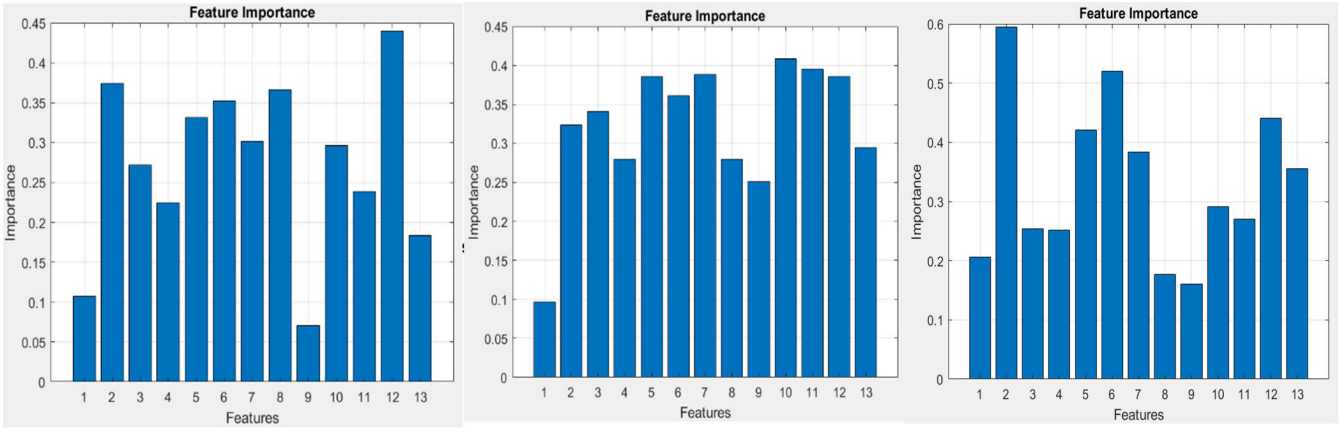

FIGURE 8. Feature importance of knee issues (a) biceps femoris subject 2, (b) semitendinosus subject 4, (c) biceps femoris subject 10.

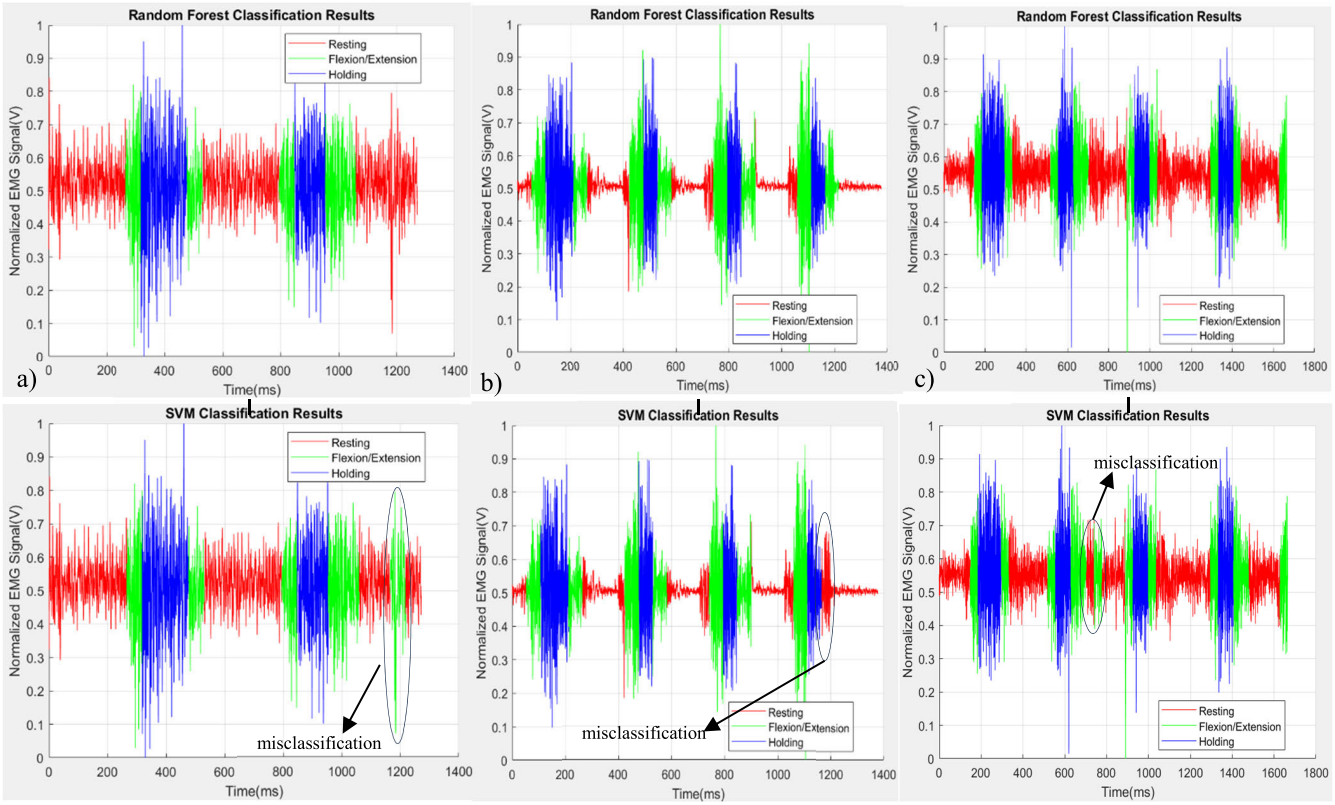

FIGURE 9. Comparison between random forest and SVM (a) biceps femoris subject 2, (b) semitendinosus subject 4, (c) biceps femoris subject 10.

and class skew, largely because of its ensemble-based logic. This reduces overfitting and enhances generalization across varied signal profiles by aggregating the outputs of the diverse decision trees. Fig. 10 shows the per-subject LOSO accuracy for the biceps femoris and semitendinosus in the SVM and Random Forest classifiers. Both models achieved robust performance, with classification accuracies consistently surpassing the 80% threshold, as shown in Fig. 10a. The extracted EMG features from the biceps femoris contain sufficient discriminative information for knee issue classification. Random Forest consistently demonstrated higher accuracy than SVM for the majority of subjects, reflecting its ability to capture nonlinear relationships and feature interactions inherent in EMG signals. Subjects S3, S5, S7, and S8 reached accuracies close to 95%, reflecting highly stable muscle activation patterns and a strong correlation between EMG features and knee movement states (Fig. 10a). Moreover, the lower accuracies for subjects S1 and S6 were caused by elevated noise levels and transient motion artifacts that obscured the underlying activation patterns. Overall, the Random Forest classifier demonstrated a performance comparable to that of the SVM for most subjects. Random forest

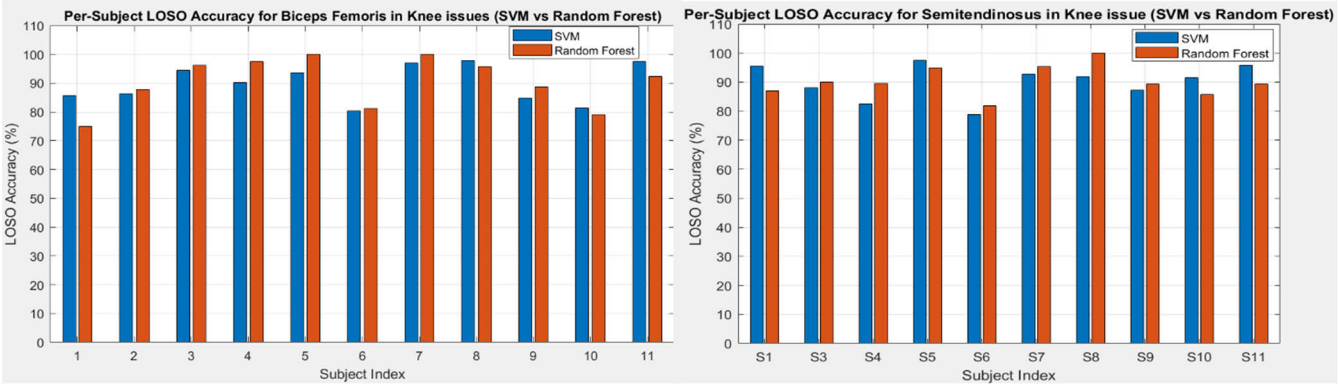

FIGURE 10. Per-subject LOSO Accuracy (a) biceps femoris (b) semitendinosus.

achieved noticeably higher accuracy for subjects S4, S6, and S8, suggesting better robustness to nonlinearity and feature interactions in the EMG signals, as shown in Fig. 10b. However, for a few subjects, such as S1 and S10, SVM marginally outperforms Random Forest, indicating that margin-based decision boundaries are still effective when EMG patterns are relatively consistent, as shown in Fig. 10b. The lower accuracy observed at S6 and S9 can be attributed to EMG noise and the weaker correspondence between muscle activation and joint kinematics. Although the knee joint angle signal remained smooth, the EMG reflected neuromuscular activation. This mismatch can lead to ambiguous feature distributions and increased misclassification.

TABLE 3. LOSO classification accuracy and MCNEMAR'S test results for SVM and random forest.

	Models	Biceps femoris	Semitendinosus
Overall classification performance accuracy	SVM	89.94% ± 6.51	90.15% ± 6.04
	Random forest	90.35% ± 8.72	90.28% ± 5.23
McNemar's test		0.8388	0.8597

Table 3 summarizes the subject-independent classification performance of the SVM and Random Forest classifiers for the biceps femoris and semitendinosus muscles using the LOSO evaluation framework. Both classifiers achieved high and comparable accuracies for both muscles. For the biceps femoris, SVM and Random Forest yielded mean accuracies of 89.94% ± 6.51 and 90.35% ± 8.72, respectively. Similarly, for the semitendinosus muscle, SVM achieved 90.15% ± 6.04, while RF achieved 90.28% ± 5.23. These results indicate that the extracted EMG features are highly informative for knee-related classification tasks and can be generalized across subjects. The results in Tables 2 and 3 are obtained using the LOSO evaluation framework. Classification accuracy is defined as the percentage of correctly classified EMG windows relative to the reference motion-phase labels. All values are reported as mean ± standard deviation across subjects. Cross-paper comparisons are inherently constrained by variations in hardware platforms, data acquisition setups, signal processing techniques, precision levels, and experimental workloads across different studies. Therefore, these comparisons should be interpreted as indicative rather than directly equivalent.

Small standard deviations indicate stable performance across individuals, even when accounting for the inherent physiological variability in EMG amplitudes between subjects. Although the Random Forest maintained a marginal lead in the mean accuracy across both muscle groups, the performance difference between the two classifiers was minimal. Both margin-based (SVM) and ensemble-based (Random Forest) learning approaches demonstrated a clear systematic advantage in terms of the overall accuracy under the LOSO evaluation. McNemar's test was conducted on the pooled LOSO predictions. McNemar's test of pooled predictions yielded p-values for the biceps femoris ($p = 0.8388$) and semitendinosus ($p = 0.8597$) muscles, that far exceeded the α threshold of 0.05. There were no statistically significant differences between the two classifiers in either muscle groups. Therefore, the null hypothesis that both models exhibit equivalent classification performances cannot be rejected.

While the Random Forest displayed superior temporal coherence to produce a more stable segmentation of motion phases in the time-series analysis, the qualitative edge did not convert into a statistically significant quantitative advantage under LOSO cross-validation. Both the SVM and Random Forest models achieved comparable mean accuracies with remarkably low inter-subject variance across the biceps femoris and semitendinosus muscle groups. Qualitative differences in time-series behavior are localized boundary artifacts that are visually distinct and exert a negligible influence on aggregate window-level accuracy metrics.

IV. CONCLUSION

This study successfully developed an EMG-based motion phase classification for subjects with and without knee issues using signals acquired from the biceps femoris and semitendinosus muscles. Signal preprocessing for the combination

of median absolute deviation-based impulsive artifact rejection with Kalman filtering suppresses transient spikes and high-frequency noise while maintaining physiological signal morphology.

Feature importance analysis indicated that classification performance was not driven by a single dominant descriptor but emerged from the synergistic contribution of multiple feature domains. However, in several subjects, standard deviation emerged as a dominant contributor, indicating that variability in muscle activation is a key discriminative factor for motion phase recognition. In addition, the RMS and higher-order autoregressive coefficients exhibited lower importance when the mean activation levels and short-term temporal dynamics were similar across motion phases. This highlights the necessity of a holistic feature set that captures both the intensity and the underlying variability of neuromuscular activity.

The Support Vector Machine reached mean LOSO accuracies of 81.79% $\pm$ 12.10 for the biceps femoris and 75.99% $\pm$ 15.58 for the semitendinosus, whereas the Random Forest achieved 88.59% $\pm$ 9.30 and 82.50% $\pm$ 13.49, respectively, for subjects without knee issues. McNemar's test confirmed a statistically significant divergence in performance ($p < 0.05$), favoring the Random Forest over the margin-based alternative. More sophisticated management of inter-subject variability and high-dimensional feature interdependence was achieved by the intrinsic stochasticity of the ensemble approach. The model produces more stable classification outputs with reduced uncertainty at the decision boundaries. This enables true resting periods to be distinguished from minimal muscle activation, a task in which traditional classifiers often struggle with class-label jitter.

Both classifiers achieved high and comparable performances for subjects with knee issues. SVM yielded mean accuracies of 89.94% $\pm$ 6.51 (biceps femoris) and 90.15% $\pm$ 6.04 (semitendinosus), whereas Random Forest achieved 90.35% $\pm$ 8.72 and 90.28% $\pm$ 5.23, respectively. McNemar's test revealed no statistically significant differences ($p > 0.05$), indicating an equivalent classification capability under the LOSO protocol. Although Random Forest produces more temporally coherent segmentation in time-series visualizations, quantitative analysis shows comparable mean accuracies and low inter-subject variability for both the biceps femoris and semitendinosus muscles. Both margin and ensemble-based learning approaches can reliably capture EMG-derived motion-phase dynamics in subjects with clearer activation patterns.

The main limitation of the current study is the sample size of the dataset, which influences the generalization to more diverse populations. Although these findings validate the feasibility of EMG-based classification for knee kinematics using the biceps femoris and semitendinosus, the scope remains restricted to the knee joint under the defined experimental protocol. The models were trained and evaluated exclusively on knee motion phases derived from joint angle measurements, and no experimental validation was conducted on other joints or multi-joint functional tasks. Therefore, conversion of this framework to holistic biomechanical analysis and knee rehabilitation systems remains an area of active investigation rather than fact.

Despite these limitations, the Random Forest model shows strong potential for application in classifying EMG signals from other muscle groups, such as the shoulder, wrist, and elbow. This enables the development of multi-joint rehabilitation and assistive systems. The results also provide a foundation for generalizing machine learning–based EMG classification methods to other biomedical signal domains.

Future research should prioritize the integration of multi-joint datasets and more varied clinical scenarios to rigorously assess the scalability and cross-joint robustness of the proposed system. Such investigations are necessary before broader clinical and assistive applications can be developed. Future research could focus on real-time EMG signal classification for integration into knee rehabilitation devices and on incorporating additional datasets to improve model reliability.

ACKNOWLEDGMENT

The authors sincerely acknowledge the Department of Electrical and Electronic Engineering, Universiti Putra Malaysia, for their valuable support throughout this research. This research was funded by the Universiti Putra Malaysia under the Putra Grant (Grant No. GP-GPB/2022/9712500).

REFERENCES

[1] K. Chaiyasit, C. Phombut, A. Wiangkham, and S. Rooppakhun, "Kinetics prediction of normal knee and undergone total knee arthroplasty during squatting based on extreme gradient boosting," *Results Eng.*, vol. 23, Sep. 2024, Art. no. 102663, doi: 10.1016/j.rineng.2024.102663.

[2] J. Abulhasan and M. Grey, "Anatomy and physiology of knee stability," *J. Funct. Morphol. Kinesiol.*, vol. 2, no. 4, p. 34, Sep. 2017, doi: 10.3390/jfmk2040034.

[3] A. Gnanaprakasam, J. M. Solomon, A. K. Roy, A. S. Deshmukh, and S. Karthikbabu, "Association between depression and adherence to upper limb exercises among community-dwelling stroke survivors: A cross-sectional study," *Health Sci. Rep.*, vol. 7, no. 10, Oct. 2024, Art. no. e70133, doi: 10.1002/hsr2.70133.

[4] E. Zvetkova, E. Koytchev, I. Ivanov, S. Ranchev, and A. Antonov, "Biomechanical, healing and therapeutic effects of stretching: A comprehensive review," *Appl. Sci.*, vol. 13, no. 15, p. 8596, Jul. 2023, doi: 10.3390/app13158596.

[5] W. Herzog, J. Sokolosky, Y. T. Zhang, and A. C. S. Guimarães, "EMG-force relation in dynamically contracting cat plantaris muscle," *J. Electromyogr. Kinesiol.*, vol. 8, no. 3, pp. 147–155, Jun. 1998, doi: 10.1016/s1050-6411(97)00015-1.

[6] Y. Chen, M. Zhang, M. Bai, and W. Chen, "Improving the signal-to-noise ratio of seismological datasets by unsupervised machine learning," *Seismological Res. Lett.*, vol. 90, no. 4, pp. 1552–1564, May 2019, doi: 10.1785/0220190028.

[7] K. E. K. Elbert, H. B. Kroemer, and A. D. K. Hoffman, "Bones, muscles, and strength of the human body," in *Ergonomics: How to Design for Ease and Efficiency*, 3rd ed., San Diego, CA, USA: Academic, 2018, pp. 11–72.

[8] M. Al-Ayyad, H. A. Owida, R. De Fazio, B. Al-Naami, and P. Visconti, "Electromyography monitoring systems in rehabilitation: A review of clinical applications, wearable devices and signal acquisition methodologies," *Electronics*, vol. 12, no. 7, p. 1520, Mar. 2023, doi: 10.3390/electronics12071520.

[9] Anatomy and Physiology. *9.10B: Muscles That Cause Movement at the Knee Joint*. Accessed: Oct. 6, 2025. [Online]. Available: https://med.libretexts.org/Bookshelves/Anatomy_and_Physiology/Anatomy_and_Physiology_(Boundless)/9%3A_Muscular_System/9.10%3A_Muscles_of_the_Lower_Limb/9.10B%3A_Muscles_that_Cause_Movement_at_the_Knee_Joint.

[10] C. D. Rodgers and A. Raja, *Anatomy, Bony Pelvis and Lower Limb, Hamstring Muscle*. Treasure Island, FL, USA: StatPearls Publishing, Jan. 2025. [Online]. Available: https://www.ncbi.nlm.nih.gov/books/NBK546688/

[11] J.-W. Seo, G.-H. Kang, C.-H. Kim, J. Jung, J. Kim, H. Kang, and S. Lee, "Characteristics of gait event and muscle activation parameters of the lower limb on the affected side in patients with hemiplegia after stroke: A pilot study," *Arch. Rehabil. Res. Clin. Transl.*, vol. 5, no. 4, Dec. 2023, Art. no. 100274, doi: 10.1016/j.arrct.2023.100274.

[12] A. D. Vigotsky, I. Halperin, G. J. Lehman, G. S. Trajano, and T. M. Vieira, "Interpreting signal amplitudes in surface electromyography studies in sport and rehabilitation sciences," *Frontiers Physiol.*, vol. 8, p. 985, Jan. 2018, doi: 10.3389/fphys.2017.00985.

[13] K. Sengchuai, C. Kanjanaroat, J. Jaruenpunyasak, C. Limsakul, W. Tayati, A. Booranawong, and N. Jindapetch, "Development of a real-time knee extension monitoring and rehabilitation system: Range of motion and surface EMG measurement and evaluation," *Healthcare*, vol. 10, no. 12, p. 2544, Dec. 2022, doi: 10.3390/healthcare10122544.

[14] M. Shi, L. Sun, Z. Bi, and R. He, "A hybrid Kalman filter and physics-informed neural network approach for leakage detection and localization in heat exchanger networks," *Comput. Chem. Eng.*, vol. 201, Oct. 2025, Art. no. 109259, doi: 10.1016/j.compchemeng.2025.109259.

[15] J. Wang, S. Lu, S.-H. Wang, and Y.-D. Zhang, "A review on extreme learning machine," *Multimedia Tools Appl.*, vol. 81, no. 29, pp. 41611–41660, Dec. 2022, doi: 10.1007/s11042-021-11007-7.

[16] N. Ádám, D. Val'ko, Z. Balogh, B. Madoš, and J. Hurtuk, "Comparative evaluation of filtration techniques for ECG signal denoising with emphasis on stationary wavelet transform," *Sci. Rep.*, vol. 15, no. 1, Nov. 2025, Art. no. 42514, doi: 10.1038/s41598-025-26476-1.

[17] K. Strzecha, M. Krakós, B. Wiécek, P. Chudzik, K. Tatar, G. Lisowski, V. Mosorov, and D. Sankowski, "Processing of EMG signals with high impact of power line and cardiac interferences," *Appl. Sci.*, vol. 11, no. 10, p. 4625, May 2021, doi: 10.3390/app11104625.

[18] M. Boyer, L. Bouyer, J.-S. Roy, and A. Campeau-Lecours, "Reducing noise, artifacts and interference in single-channel EMG signals: A review," *Sensors*, vol. 23, no. 6, p. 2927, Mar. 2023, doi: 10.3390/s23062927.

[19] I. Christov, R. Raikova, and S. Angelova, "Separation of electrocardiographic from electromyographic signals using dynamic filtration," *Med. Eng. Phys.*, vol. 57, no. 1, pp. 1–10, Jul. 2018, doi: 10.1016/j.medengphy.2018.04.007.

[20] H. Tankisi, D. Burke, L. Cui, M. de Carvalho, S. Kuwabara, S. D. Nandedkar, S. Rutkove, E. Stålberg, M. J. A. M. van Putten, and A. Fuglsang-Frederiksen, "Standards of instrumentation of EMG," *Clin. Neurophysiol.*, vol. 131, no. 1, pp. 243–258, Jan. 2020, doi: 10.1016/j.clinph.2019.07.025.

[21] D. C. Toledo-Pérez, J. Rodríguez-Reséndiz, R. A. Gómez-Loenzo, and J. C. Jauregui-Correa, "Support vector machine-based EMG signal classification techniques: A review," *Appl. Sci.*, vol. 9, no. 20, p. 4402, Oct. 2019, doi: 10.3390/app9204402.

[22] C. L. Kok, C. K. Ho, F. K. Tan, and Y. Y. Koh, "Machine learning-based feature extraction and classification of EMG signals for intuitive prosthetic control," *Appl. Sci.*, vol. 14, no. 13, p. 5784, Jul. 2024, doi: 10.3390/app14135784.

[23] C. Mokri, M. Bamdad, and V. Abolghasemi, "Muscle force estimation from lower limb EMG signals using novel optimised machine learning techniques," *Med. Biol. Eng. Comput.*, vol. 60, no. 3, pp. 683–699, Mar. 2022, doi: 10.1007/s11517-021-02466-z.

[24] L. Moreira, J. Figueiredo, P. Fonseca, J. P. Vilas-Boas, and C. P. Santos, "Lower limb kinematic, kinetic, and EMG data from young healthy humans during walking at controlled speeds," *Sci. Data*, vol. 8, no. 1, Apr. 2021, Art. no. 103, doi: 10.1038/s41597-021-00881-3.

[25] M. T. N. Truong, A. E. A. Ali, D. Owaki, and M. Hayashibe, "EMG-based estimation of lower limb joint angles and moments using long short-term memory network," *Sensors*, vol. 23, no. 6, p. 3331, Mar. 2023, doi: 10.3390/s23063331.

[26] R. V. Schulte, E. C. Prinsen, L. Schaake, R. P. G. Paassen, M. Zondag, E. S. van Staveren, M. Poel, and J. H. Buurke, "Database of lower limb kinematics and electromyography during gait-related activities in able-bodied subjects," *Scientific Data*, vol. 10, no. 1, Jul. 2023, Art. no. 461, doi: 10.1038/s41597-023-02341-6.

[27] M. Atzori, A. Gijsberts, I. Kuzborskij, S. Elsig, A.-G. M. Hager, O. Deriaz, C. Castellini, H. Müller, and B. Caputo, "Characterization of a benchmark database for myoelectric movement classification," *IEEE Trans. Neural Syst. Rehabil. Eng.*, vol. 23, no. 1, pp. 73–83, Jan. 2015, doi: 10.1109/TNSRE.2014.2328495.

[28] M. Findik, S. Yilmaz, and M. Koseoglu, "Random forest classification of finger movements using electromyogram (EMG) signals," in *Proc. IEEE Sensors*, Rotterdam, The Netherlands, Oct. 2020, pp. 1–4, doi: 10.1109/SENSORS47125.2020.9278619.

[29] R. Meattini, S. Benatti, U. Scarcia, D. De Gregorio, L. Benini, and C. Melchiorri, "An sEMG-based human–robot interface for robotic hands using machine learning and synergies," *IEEE Trans. Compon., Packag., Manuf. Technol.*, vol. 8, no. 7, pp. 1149–1158, Jul. 2018, doi: 10.1109/TCPMT.2018.2799987.

[30] Z. Fu, A. Y. Bani Hashim, Z. Jamaludin, and I. S. Mohamad, "Review on EMG acquisition and classification techniques: Towards zero retraining in the influence of user and arm position independence," *Int. J. Integr. Eng.*, vol. 13, no. 4, pp. 1–15, May 2021, doi: 10.30880/ijie.2021.13.04.001.

[31] L. Piyathilaka, J.-H. Sul, S. D. Arachchige, A. Jayawardena, and D. Moratuwage, "Advances in EMG signal processing and pattern recognition: Techniques, challenges, and emerging applications," *Electronics*, vol. 15, no. 3, p. 590, Jan. 2026, doi: 10.3390/electronics15030590.

[32] J. M. Lopez-Villagomez, J. M. Lopez-Hernandez, R. I. Mata-Chavez, C. Rodriguez-Donate, Y. Guzman-Castro, and E. Cabal-Yepez, "Comparative evaluation of EMG signal classification techniques across temporal, frequency, and time-frequency domains using machine learning," *Appl. Sci.*, vol. 16, no. 2, p. 1058, Jan. 2026, doi: 10.3390/app16021058.

[33] P. Mukherjee and A. Halder Roy, "A deep learning-based comprehensive robotic system for lower limb rehabilitation," *Biomed. Signal Process. Control*, vol. 100, Feb. 2025, Art. no. 107178, doi: 10.1016/j.bspc.2024.107178.

[34] Y. Wu, X. Hu, Z. Wang, J. Wen, J. Kan, and W. Li, "Exploration of feature extraction methods and dimension for sEMG signal classification," *Appl. Sci.*, vol. 9, no. 24, p. 5343, Dec. 2019, doi: 10.3390/app9245343.

[35] A. Phinyomark, R. N. Khushaba, and E. Scheme, "Feature extraction and selection for myoelectric control based on wearable EMG sensors," *Sensors*, vol. 18, no. 5, p. 1615, May 2018, doi: 10.3390/s18051615.

[36] K. Nurhanim, I. Elamvazuthi, L. I. Izhar, G. Capi, and S. Su, "EMG signals classification on human activity recognition using machine learning algorithm," in *Proc. 8th NAFOSTED Conf. Inf. Comput. Sci. (NICS)*, Dec. 2021, pp. 369–373, doi: 10.1109/NICS54270.2021.9701461.

[37] S. Abbaspour, M. Lindén, H. Gholamhosseini, A. Naber, and M. Ortiz-Catalan, "Evaluation of surface EMG-based recognition algorithms for decoding hand movements," *Med. Biol. Eng. Comput.*, vol. 58, no. 1, pp. 83–100, Jan. 2020, doi: 10.1007/s11517-019-02073-z.

[38] A. Sultana, F. Ahmed, and M. S. Alam, "A systematic review on surface electromyography-based classification system for identifying hand and finger movements," *Healthcare Analytics*, vol. 3, Nov. 2023, Art. no. 100126, doi: 10.1016/j.health.2022.100126.

[39] A. Phinyomark, C. Limsakul, and P. Phukpattaranont, "Application of wavelet analysis in EMG feature extraction for pattern classification," *Meas. Sci. Rev.*, vol. 11, no. 2, pp. 45–52, Jan. 2011, doi: 10.2478/v10048-011-0009-y.

[40] H. Li, G. Zhao, Y. Zhou, X. Chen, Z. Ji, and L. Wang, "Relationship of EMG/SMG features and muscle strength level: An exploratory study on tibialis anterior muscles during plantar-flexion among hemiplegia patients," *Biomed. Eng. OnLine*, vol. 13, no. 1, Dec. 2014, Art. no. 5, doi: 10.1186/1475-925x-13-5.

[41] M. Bodruzzaman, M. Wilkes, R. Shiavi, and A. Kilroy, "Classification of electromyographic signals by autoregressive modeling," in *IEEE Proc. Southeastcon*, vol. 2, New Orleans, LA, USA, Apr. 1990, pp. 508–510, doi: 10.1109/SECON.1990.117866.

[42] J.-H. Sul, L. Piyathilaka, D. Moratuwage, S. D. Arachchige, A. Jayawardena, G. Kahandawa, and D. M. G. Preethichandra, "Electromyography signal acquisition, filtering, and data analysis for exoskeleton development," *Sensors*, vol. 25, no. 13, p. 4004, Jun. 2025, doi: 10.3390/s25134004.

[43] L.-L. Li, G.-Z. Cao, H.-J. Liang, Y.-P. Zhang, and F. Cui, "Human lower limb motion intention recognition for exoskeletons: A review," *IEEE Sensors J.*, vol. 23, no. 24, pp. 30007–30036, Dec. 15, 2023, doi: 10.1109/JSEN.2023.3328615.

[44] Y. Omama, C. Haddad, M. Machaalany, A. Hamoudi, M. Hajj-Hassan, M. A. Ali, and L. Hamawy, "Surface EMG classification of basic hand movement," in *Proc. 5th Int. Conf. Adv. Biomed. Eng. (ICABME)*, Tripoli, Lebanon, Oct. 2019, pp. 1–4, doi: 10.1109/ICABME47164.2019.8940352.

[45] O. Sanchez and J. Sotelo, "EMG dataset in lower limb," UCI Mach. Learn. Repository, USA, 2014, doi: 10.24432/C5ZW3P.

[46] P. Tu, J. Li, and H. Wang, "Lower limb motion recognition with improved SVM based on surface electromyography," *Sensors*, vol. 24, no. 10, p. 3097, May 2024, doi: 10.3390/s24103097.
[47] E. R. Avila, S. E. Williams, and C. Disselhorst-Klug, "Advances in EMG measurement techniques, analysis procedures, and the impact of muscle mechanics on future requirements for the methodology," *J. Biomechanics*, vol. 156, Jul. 2023, Art. no. 111687, doi: 10.1016/j.jbiomech.2023.111687.

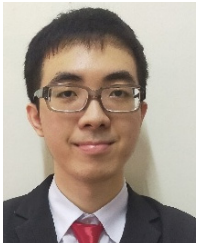

ING TECK PHANG received the B.Eng. degree in electrical and electronic engineering from the Universiti Putra Malaysia (UPM), Serdang, Malaysia, in 2023, where he is currently pursuing the master's degree in control system engineering. His major field of study includes control systems, power systems, and biotechnology systems. His current research focuses on electromyography (EMG)-based control systems, machine learning for signal classification, and the development of intelligent lower-limb rehabilitation devices.

ASNOR JURAIZA ISHAK (Senior Member, IEEE) received the bachelor's degree in electrical-mechatronic engineering from the University of Technology Malaysia (UTM), the M.Sc. degree in control automation system engineering from the Universiti Putra Malaysia (UPM), and the Ph.D. degree in electrical, electronic, and system engineering from the Universiti Kebangsaan Malaysia (UKM). She is currently an Associate Professor with the Department of Electrical and Electronic Engineering, UPM. Her research interests include artificial intelligence, predictive modeling, control systems, rehabilitation and assistive robotics, and digital twins. She is a member of the International Association of Engineers and the Board of Engineers Malaysia.

SITI ANOM AHMAD (Senior Member, IEEE) received the B.Eng. degree in electronic/computer from the Universiti Putra Malaysia (UPM), in 1999, and the M.Sc. degree in microelectronics system design and the Ph.D. degree in electronics from the University of Southampton, U.K., in 2004 and 2009, respectively. She is currently a Professor with the Faculty of Engineering, UPM. Her research interests include biomedical engineering, artificial intelligence, gerontechnology, and intelligent control systems. She is a Professional Engineer of the Board of Engineers Malaysia, a Chartered Engineer of the Institute of Engineering and Technology (IET), and a member of the Institute of Engineers Malaysia (IEM).

TOMOHIRO SHIBATA (Member, IEEE) received the B.E. degree in mechanical engineering and the M.E. and Ph.D. degrees in information engineering from The University of Tokyo, Tokyo, Japan, in 1991, 1993, and 1996, respectively. He is currently a Professor with the Graduate School of Life Science and Systems Engineering, Kyushu Institute of Science and Technology, Japan. His main research interests include understanding and assisting motor control and decision-making by humans by using interdisciplinary approaches. He is a member of the IEEE Robotics and Automation Society, the IEEE Computational Intelligence Society, the Robotics Society of Japan, the Robotics Society of India, the Institute of Electronics, Information and Communication Engineers, and the Japanese Neural Network Society.

SLAMET RIYADI (Member, IEEE) received the bachelor's degree in electrical engineering from Universitas Gadjah Mada, Indonesia, and the M.Sc. and Ph.D. degrees from the Department of Electrical, Electronic, and Systems Engineering, National University of Malaysia. He is currently the Vice Rector of the Universitas Muhammadiyah Yogyakarta (UMY) and an Associate Professor with the Department of Information Technology. He has authored over 80 scientific publications in national and international journals, including recent works on the application of machine learning in medicine. His research interests include artificial intelligence, machine learning, computer vision, and image processing. He has served as a reviewer and an editor at several conferences and journals.